

## pH-Dependent Electrochemically Catalyzed Oxygen Reduction Behaviors of o-Substituted Co(III) Corroles

Wei Tang,<sup>a</sup> Yuanyuan Qiu,<sup>b</sup> Xiaonan Li,<sup>a@1</sup> Rodah C. Soy,<sup>c</sup> John Mack,<sup>c@2</sup> Tebello Nyokong,<sup>c</sup> and Xu Liang<sup>b@3</sup>

<sup>a</sup>Department of Children Health Care, Nanjing Children's Hospital, Nanjing Medical University, 210008 Nanjing, PR China

<sup>b</sup>School of Chemistry and Chemical Engineering, Jiangsu University, 212013 Zhenjiang, PR China

<sup>c</sup>Institute for Nanotechnology Innovation, Department of Chemistry, Rhodes University, 6140 Makhanda, South Africa

@1 Corresponding author E-mail: [xiaonan6189@163.com](mailto:xiaonan6189@163.com)

@2 Corresponding author E-mail: [j.mack@ru.ac.za](mailto:j.mack@ru.ac.za)

@3 Corresponding author E-mail: [Liangxu@ujs.edu.cn](mailto:Liangxu@ujs.edu.cn)

*Herein, a series of three o-substituted Co(III) corroles with electron-donating/withdrawing moieties have been prepared and fully characterized. The different functional substituents at o-position of meso-phenyl rings results in tunable local environment, and unusual pH-dependent electrochemically catalyzed oxygen reduction behaviors were clearly observed.*

**Keywords:** Co(III) corroles, local environment, electrochemistry, TD-DFT calculations, oxygen reductions.

## pH-Зависимое электрохимически катализируемое окислительно-восстановительное поведение o-замещенных Co(III) корролов

В. Танг,<sup>a</sup> Ю. Киу,<sup>b</sup> К. Ли,<sup>a@1</sup> Р. Сой,<sup>c</sup> Дж. Мак,<sup>c@2</sup> Т. Ниоконг,<sup>c</sup> К. Лианг<sup>b@3</sup>

<sup>a</sup>Отдел детского здравоохранения, Нанкинская детская больница, Нанкинский медицинский университет, 210008 Нанкин, Китай

<sup>b</sup>Школа химии и химической инженерии, Университет Цзянсу, 212013 Чжэньцзян, Китай

<sup>c</sup>Институт инноваций в области нанотехнологии, кафедра химии, Университет Родса, 6140 Маканда, ЮАР

@1 E-mail: [xiaonan6189@163.com](mailto:xiaonan6189@163.com)

@2 E-mail: [j.mack@ru.ac.za](mailto:j.mack@ru.ac.za)

@3 E-mail: [Liangxu@ujs.edu.cn](mailto:Liangxu@ujs.edu.cn)

*В работе были получены и полностью охарактеризованы три o-замещенных Co(III)-коррола с электронодонорными/электроноакцепторными фрагментами. Различные функциональные группы в o-положении мезо-фенильных колец приводят к локальным изменениям, отчетливо наблюдалось необычное pH-зависимое электрохимически катализируемое окислительно-восстановительное поведение.*

**Ключевые слова:** Co(III)-корролы, локальное окружение, электрохимия, TD-DFT расчеты, восстановление кислорода.

## Introduction

Earth-abundant first row transition metal corrole complexes have played an important role in fundamental research due to their unique molecular structures and attractive properties.<sup>[1–4]</sup> In comparison to porphyrins, corroles have three inner N-H protons and are ring-contracted with a smaller macrocyclic cavity.<sup>[5–6]</sup> First row transition metal corroles have been widely used as effective electrochemical catalysts for small molecule activations, such as hydrogen evolution, oxygen reduction/evolution and CO<sub>2</sub> reduction reactions (HERs, ORRs/OERs and CO<sub>2</sub>RRs) through homogenous and/or heterogenous procedures.<sup>[7–10]</sup> Several strategies have been used to modulate the catalytic efficiency of synthetic metalcorroles. For example, the introduction of functional substituents at the *meso*- and/or  $\beta$ -positions of metalcorroles rings can be used to enhance the catalytic efficiency, through perturbation to the electronic structure of the complexes.<sup>[11–14]</sup> Research has also focused on modulating the electron transfer properties between the catalytic center of metal corroles and carbon supports.<sup>[15–18]</sup> Metalcorrole based covalent organic frameworks have been also prepared through chemical and/or electrochemical polymerization to obtain highly efficient catalysts.<sup>[19–20]</sup> Interestingly, the super-structure of metalcorroles have also been reported to enhance their electrochemical catalysts. For example, the introduction of a “hangman” ligand enables the precise control of the placement of a proton-donating or -accepting moiety over the face of a macrocyclic redox site.<sup>[21–24]</sup> Thus, it is reasonable to assume that changes to the local environment of metalcorroles could be an effective strategy for enhancing the catalytic efficiency. According to the crystal structures of Co(III)PPh<sub>3</sub>-triarylcorrole, *o*- and *m*-functional units of *meso*-phenyl rings generally lie at the distal side of the corrole rings due to steric hindrance related to the triphenylphosphine ligands. Herein, we describe how *o*-substituted Co(III)-triarylcorroles modulate electrochemically catalyzed oxygen reductions, by combining electrochemical studies with an analysis of the trends in the optical spectra and TD-DFT calculations will also be described.

## Experimental

*Synthesis of Co(III)-5,10,15-triphenylcorroles (3a).* The general experimental procedures are described in the Supporting

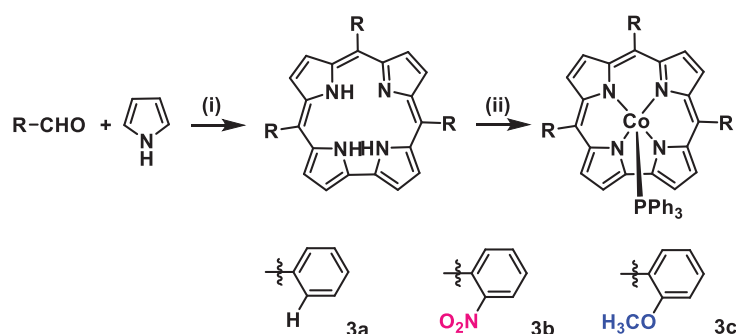
information. The Co(III)PPh<sub>3</sub>-corroles were synthesized through a metal-insertion reaction of the corresponding free base corroles (0.05 mmol) by using excess cobalt acetate (0.25 mmol) and triphenylphosphine dissolved in 25 mL of CH<sub>2</sub>Cl<sub>2</sub>/CH<sub>3</sub>OH (v/v = 1:4) solution at 75 °C under N<sub>2</sub> for 1 h. After removal of the solvent on a rotary evaporator, the crude product was purified by silica gel column chromatography and recrystallized. Free base corrole **2a** was prepared according to literature procedure.<sup>[25]</sup> The target *o*-substituted Co(III)-corrole **3a** was obtained as deep-red solid state compound in a 55.6 % yield (0.047 g). MALDI-TOF: *m/z* = 843.29 (Calcd. [M-PPh<sub>3</sub>]<sup>+</sup> = 844.84). IR (KBr)  $\nu_{\max}$  cm<sup>-1</sup>: 3424 s, 3053 w, 2972 w, 2924 w, 2364 w, 1597 m, 1571 w, 1556 w, 1535 w, 1504 m, 1433 s, 1344 m, 1318 m, 1223 w, 1175 w, 1088 w, 1070 w, 1052 vs, 1015 s, 984 m, 881 w, 843 w, 787 m, 747 s, 715 s, 699 s, 669 w, 521 vs. <sup>1</sup>H NMR (400 MHz, CDCl<sub>3</sub>)  $\delta_{\text{H}}$  ppm: 8.58 (2H, d, *J* = 4.2 Hz), 8.32 (2H, d, *J* = 4.5 Hz), 8.15–8.03 (4H, d, *J* = 4.0 Hz), 7.99 (3H, s), 7.72–7.48 (11H, m), 7.41–7.31 (1H, d, *J* = 7.0 Hz), 7.05 (3H, t, *J* = 7.2 Hz), 6.76–6.64 (6H, t, *J* = 6.9 Hz), 4.72 (6H, dd, *J*<sub>1</sub> = 9.8 Hz, *J*<sub>2</sub> = 8.4 Hz).

*Synthesis of Co(III)-5,10,15-tri(o-nitrophenyl)corrole (3b).* The general synthetic procedure is same as that for **3a**, with the exception that *o*-nitrobenzaldehyde was used. The target compound was successfully obtained in a 64.5 % yield (0.0320 g). MALDI-TOF: *m/z* = 979.64 (Calcd. [M-PPh<sub>3</sub>]<sup>+</sup> = 979.83). IR (KBr)  $\nu_{\max}$  cm<sup>-1</sup>: 3444 s, 3056 w, 2358 w, 1733 w, 1652 w, 1606 w, 1570 w, 1558 w, 1526 vs, 1456 w, 1436 m, 1353 vs, 1320 w, 1260 w, 1224 w, 1161 w, 1052 m, 1016 m, 984 m, 874 w, 847 m, 787 m, 741 s, 716 s, 693 s, 666 w, 521 s. <sup>1</sup>H NMR (400 MHz, CDCl<sub>3</sub>)  $\delta_{\text{H}}$  ppm: 8.72–8.61 (1H, dd, *J*<sub>1</sub> = 37.4 Hz, *J*<sub>2</sub> = 4.3 Hz), 8.46–8.37 (1H, m), 8.33–8.15 (5H, m), 8.11 (1H, d, *J* = 4.8 Hz), 8.08–7.98 (2H, dd, *J*<sub>1</sub> = 12.8 Hz, *J*<sub>2</sub> = 6.2 Hz), 7.98–7.88 (2H, m), 7.87–7.66 (6H, m), 7.62 (1H, t, *J* = 7.1 Hz), 7.03 (3H, t, *J* = 7.2 Hz), 6.73 (6H, m), 4.91–4.66 (6H, m).

*Synthesis of Co(III)-5,10,15-tri(o-methoxyphenyl)corrole (3c).* The general synthetic procedure is same as that for **3a**, with the exception that *o*-methoxybenzaldehyde was used. The target compound was successfully obtained in a 62.3 % yield (0.0289 g). MALDI-TOF: *m/z* = 933.42 (Calcd. [M-PPh<sub>3</sub>]<sup>+</sup> = 934.92). IR (KBr)  $\nu_{\max}$  cm<sup>-1</sup>: 3442 s, 3057 w, 2927 w, 2829 w, 2359 w, 2324 w, 1643 m, 1575 w, 1536 w, 1488 m, 1457 m, 1432 s, 1344 w, 1317 m, 1286 w, 1248 s, 1158 w, 1117 m, 1047 s, 1017 s, 983 m, 855 w, 787 m, 750 s, 711 m, 660 w, 618 w, 521 s. <sup>1</sup>H NMR (400 MHz, CDCl<sub>3</sub>)  $\delta_{\text{H}}$  ppm: 8.37 (1H, m), 8.17 (1H, d, *J* = 30.4 Hz), 8.10–7.81 (5H, m), 7.80–7.41 (8H, m), 7.23–7.10 (4H, m), 7.08–6.95 (4H, m), 6.76–6.60 (6H, m), 4.99–4.72 (6H, m), 3.64–3.43 (7H, m), 3.27 (2H, d, *J* = 6.0 Hz).

## Results and Discussion

Free base corroles (**2a–c**) were synthesized according to literature procedures from a reaction of dipyrromethane **1** and an arylaldehyde (Scheme 1).<sup>[25]</sup> Co(III)-Triarylcorroles (**3a–c**) were then synthesized by a metal-insertion



**Scheme 1.** Synthetic procedure of *o*-substituted Co(III)-corroles **3**.

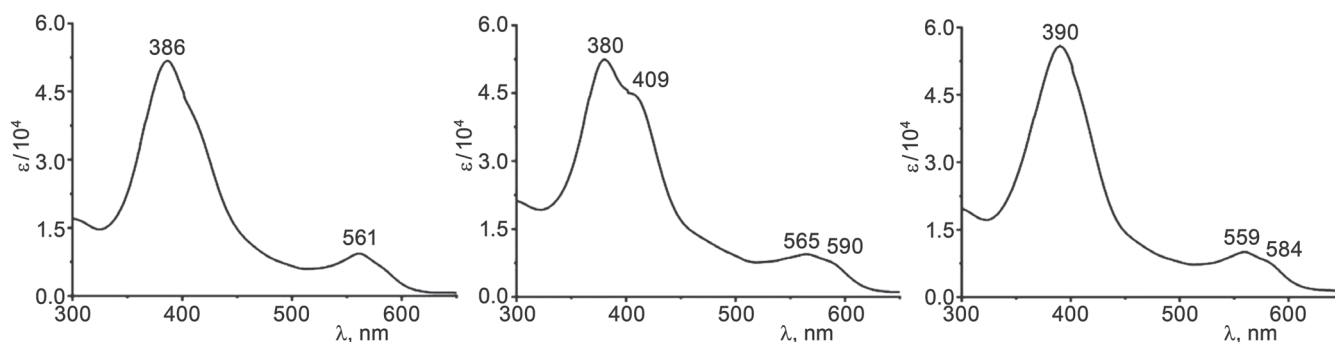


**Figure 1.** The UV-Visible absorption spectra of **3a-c** in  $\text{CH}_2\text{Cl}_2$ .

reaction of **2a-c** by using excess cobalt acetate and triphenylphosphine, and were purified by silica gel column chromatography and recrystallized. MALDI-TOF MS for **3a** revealed an intense parent peak at  $m/z = 843.29$  (Calcd.  $[\text{M-PPh}_3]^+ = 844.84$ ), providing direct evidence that the Co(III)-triphenylcorrole **3a** target compound was successfully prepared. Similar parent peaks were observed for **3b** and **3c**. In the  $^1\text{H}$  NMR spectra of **3a-c**, the proton signals for both the *meso*-substituents and pyrrole rings lie beyond 7.40 ppm and the other three signals at 7.10, 6.70 and 4.50 ppm can be assigned to the triphenylphosphine axial ligand (Figure S1, see ESI). The peaks from 3056 and 2970  $\text{cm}^{-1}$ , and at 1608 and 1490  $\text{cm}^{-1}$  in the FT-IR spectra, can be assigned to C-H stretching and benzene skeleton vibrations, respectively. The peaks at 1526 and 1353  $\text{cm}^{-1}$ , and at 1248 and 1117  $\text{cm}^{-1}$  can be assigned, respectively, to the  $-\text{NO}_2$  and  $-\text{OMe}$  groups of Co(III)PPh<sub>3</sub> corroles **3b** and **3c** (Figure S2, see ESI).

The electronic structures of the  $\pi$ -systems of porphyrinoids and their optical spectra (Figures 1 and 2) can be readily understood by using Gouterman's 4-orbital model<sup>[26]</sup> and Michl's perimeter model<sup>[27]</sup> as conceptual frameworks through a consideration of how different structural perturbations alter the energies of the frontier  $\pi$ -molecular orbitals ( $\pi$ -MOs) of a parent hydrocarbon perimeter.<sup>[28]</sup> The  $\pi$ -MOs of the  $\text{C}_{15}\text{H}_{15}^{3-}$  parent perimeter of corroles are arranged in an  $M_L = 0, \pm 1, \pm 2, \pm 3, \pm 4, \pm 5, \pm 6, \pm 7$  sequence in ascending energy terms due to their angular nodal properties. The highest occupied and lowest occupied molecular orbitals (HOMO and LUMO) have  $M_L$  values of  $\pm 4$  and  $\pm 5$ , respectively. Michl<sup>[27]</sup> introduced an **a**, **s**, **-a**, **-s** nomenclature (Figure 3) for the MOs that are derived from the HOMO (**a**, **s**) and LUMO (**-a**, **-s**) of the parent perimeter depending on whether a nodal plane is aligned with the  $z$ -axis (**a**, **-a**) or there are large MO coefficients (**s**, **-s**). When the UV-Visible absorption spectra of **3a-c** (Figure 1) are compared to analogous bands in the spectra of Co(III)-triarylcorroles,<sup>[10]</sup> the introduction of electron-withdrawing *o*-nitrophenyl and donating *o*-methoxyphenyl substituents at *meso*-positions results in only minor-shifts of the *Q*-bands (**3a**: 561 and 584 nm, **3b**: 565 and 590 nm, and **3c**: 559 and 584 nm). The only significant spectral differences that are observed are related to a splitting of the *B*-band of Co(III)-corrole **3b**. TD-DFT calculations demonstrate that this can be assigned

to the presence of weak transitions into MOs localized on the *meso*-aryl rings (Figures 2 and 3 and Table S1, see ESI). The MO energy structures of **3a-c**, only differ based on the weak inductive effect of the *meso*-aryl groups. The introduction of electron-withdrawing and -donating groups at the *o*-positions of **3b** and **3c** results in a uniform stabilization or destabilization of the  $\pi$ -MO energies and the HOMO-LUMO gaps remain almost unchanged (Figures 2 and 3).

To gain further insight into the electronic structures and redox properties of **3a-c**, cyclic and differential pulse voltammetry (CV and DPV) measurements were carried

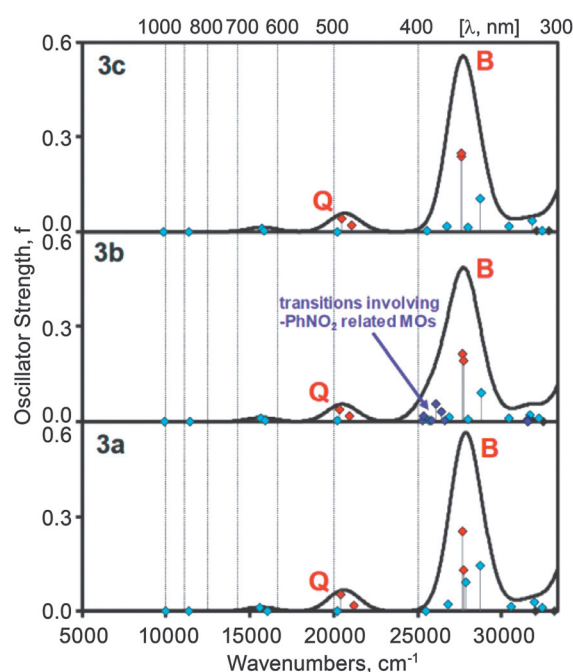


**Figure 2.** The TD-DFT calculations of **3a-c** at the CAM-B3LYP/6-31G(d) level of theory. The *Q*- and *B*-bands that are associated with the main spin-allowed transitions between the **a**, **s**, **-a** and **-s** MOs of Michl's perimeter model are highlighted with red diamonds and blue diamonds are used to highlight transitions associated with the  $3d$  orbitals of the central Co(III) ion. Purple and black diamonds are used to highlight transitions into three MOs localized on the *meso*-aryl groups due to the presence of the nitro groups and other  $\pi \rightarrow \pi^*$  transitions, respectively.

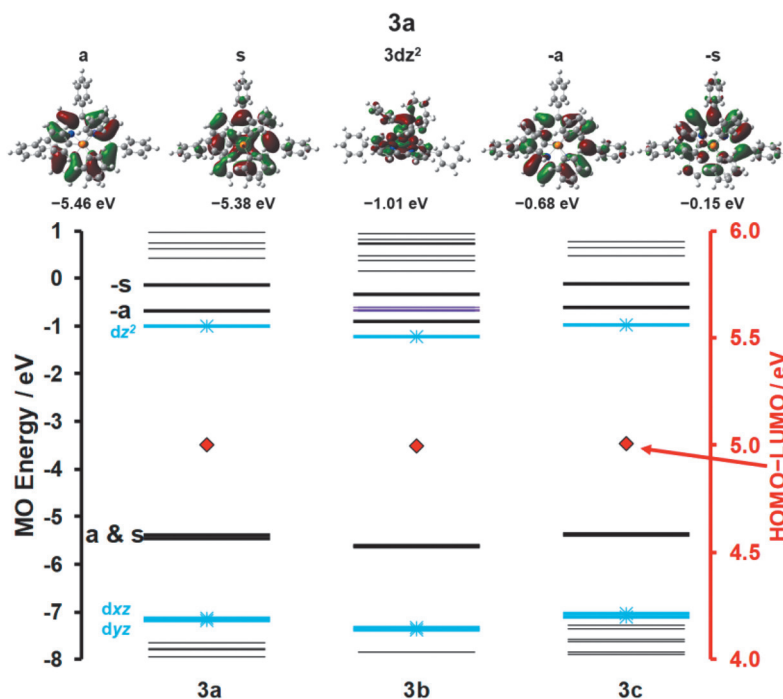


**Figure 3.** The MO energies of **3a-c** at the CAM-B3LYP/6-31G(d) level of theory (bottom). The **a**, **s**, **-a** and **-s** MOs of Michl's perimeter model are highlighted with thicker black lines and the  $3d$  orbitals of the central Co(III) ion are highlighted and blue with stars. MOs associated with the *meso*-aryl groups of **3b** that lie between the **-a** and **-s** MOs are highlighted in purple. Red diamonds are used to highlight the HOMO–LUMO gaps which are plotted against a secondary axis. The angular nodal patterns of the **a**, **s**, **-a**, **-s** and  $3d_{z^2}$  MOs of **3a** are shown at an isosurface of 0.02 a.u. (top).

out in *o*-dichlorobenzene (*o*-DCB), so that redox potential ( $E_{1/2}$ ) values could be clearly derived (Figure 4 and Table 1). The effect of reduction is more complex, however, due to the presence of a  $3d$  orbital associated with the central Co(III) ion and two MOs associated with the *meso*-nitrophenyl rings in addition to the **-a** and **-s** MOs. Co(III)-Corroles have been reported to undergo a facile one-electron reduction to generate a  $[\text{Co(II)corrole}]^-$  species together with the removal of axial  $\text{PPh}_3$  ligand during the first reduction step, followed by a one-electron reduction on the rings and at the metal center as the second and third steps (sometimes the reduction of the *meso*-substituents is also observed, for example with the nitrophenyl-unit of **3a**), respectively. While there is a positive shift of the oxidation curves and a negative shift of the reduction curves when the redox data of electron-deficient **3b** are compared to those for Co(III)-triphenylcorrole **3a**, and the potential values of electron-rich Co(III)-corrole **3c** were negatively shifted (Figure 4, Table 1). The poorly defined cathodic reduction peak and the negative shifts of the  $E_{1/2}$  value for the Co(III)/Co(II) processes are mainly caused by the loss

of the  $\text{PPh}_3$  axial ligand and an associated reaction due to electron transfer. The trend observed in the gaps between the first reduction and oxidation steps is consistent with the slight blue shift of the main *B*-band that is observed spectroscopically for the compound with more strongly electron-withdrawing *meso*-aryl rings.

The Co(III)-triarylcorrole/rGO (Co(III) $\text{PPh}_3$ -triarylcorrole/rGO-graphene) composites were examined as electrocatalysts for use in ORRs, and the stability of the Co(III)-corroles in both strongly acidic and strong base media was confirmed by using previously reported procedures.<sup>[10]</sup> The next step was to confirm the pH effect on the ORRs catalysed by Co(III)-triarylcorrole/rGO composites. Catalyst-loaded GCEs were immersed in 0.5 M  $\text{H}_2\text{SO}_4$  solution and in 0.1 M NaOH for the ORR measurements (Figure 5). In strongly acidic media ( $\text{pH} = 1$ ), the onset potentials of Co(III)-corroles **3a-c** under an  $\text{O}_2$  atmosphere were arranged at 0.493 V for **3c**, 0.498 V for **3b**, and 0.508 V for **3a** (Table 2). When the pH value increased to 4.0, the order of onset potentials changed to **3a** (0.474 V) > **3b** (0.448 V) > **3c** (0.419 V). When Co(III)-corroles **3a-c** were

**Table 1.** Potential values ( $E_{1/2}$ , V) of Co(III)-corroles **3a-c**.

	$E_{1/2}$ Ox II	$E_{1/2}$ Ox I	$E_{1/2}$ Red I	$E_{1/2}$ Red II	$E_{1/2}$ Red III
<b>3a</b>	1.10	0.60	-0.58	-1.55	–
<b>3b</b>	1.18	0.73	-0.50	-1.24	-1.37
<b>3c</b>	1.12	0.48	-0.67	-1.66	–

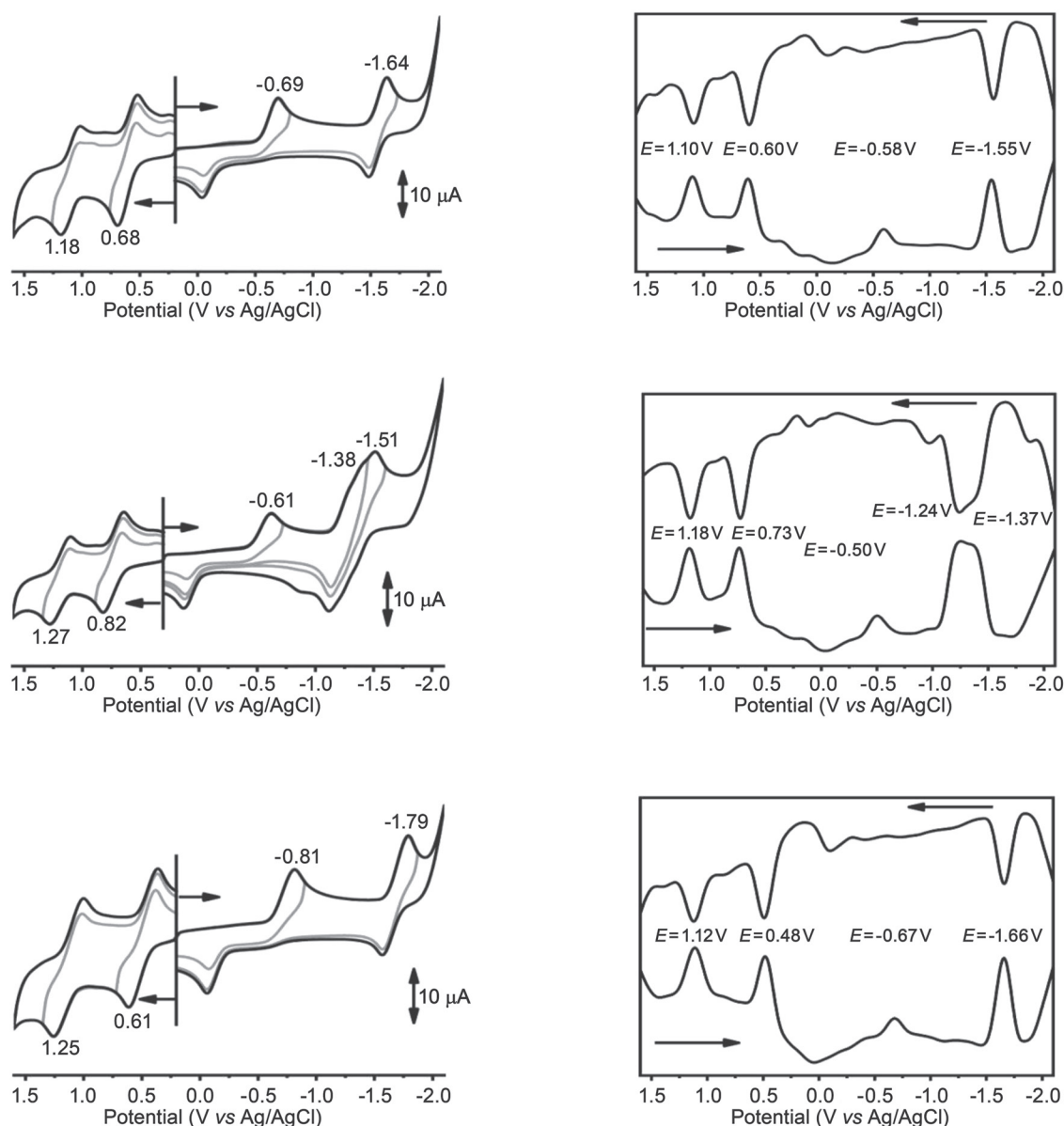


**Figure 4.** CV (left) and DPV (right) measurements of **3a** (top), **3b** (middle) and **3c** (bottom) in *o*-DCB containing 0.1 M TBAP.

**Table 2.** Active potentials of electrochemically catalyzed oxygen reductions of **3a-c** at different pH values.

pH value	1st	2nd	3rd
1.0	<b>3a</b> (0.508 V)	<b>3c</b> (0.498 V)	<b>3b</b> (0.493 V)
4.0	<b>3a</b> (0.474 V)	<b>3b</b> (0.448 V)	<b>3c</b> (0.419 V)
7.0	<b>3b</b> (0.475 V)	<b>3a</b> (0.432 V)	<b>3c</b> (0.427 V)
10.0	<b>3b</b> (0.601 V)	<b>3a</b> (0.579 V)	<b>3c</b> (0.565 V)
13.0	<b>3b</b> (0.795 V)	<b>3c</b> (0.784 V)	<b>3a</b> (0.769 V)

tested in the neutralized and basic media, Co(III)-corroles **3b**, with *o*-nitrophenyl substituents, revealed better performance on the electrochemically catalyzed oxygen reductions. The active potentials vs pH relationship is shown in Figure 6. Considering **3b** has an electron-withdrawing *o*-nitrophenyl unit, the interactions between the O<sub>2</sub> molecule

and the catalytic Co(III) center in negative OH<sup>-</sup> charge abundant media (pH > 7) must be stronger than for the other complexes. Thus, the electrochemically catalyzed oxygen reduction could be enhanced. Meanwhile, **3c** with the electron-donating *o*-methoxyphenyl group, has a better performance in H<sup>+</sup> positive charge abundant media (pH = 1). It is clear from the investigation of the electronic structures of the Co(III)-triarylcorroles that the introduction of *o*-functionalized Co(III)PPh<sub>3</sub>-corroles has a minor effect, thus the tuneable electrocatalytic properties can be assigned to the change of local environment of the catalytic center of Co(III)PPh<sub>3</sub>-corroles **3a-c**.

## Conclusions

A series of three *o*-substituted Co(III)-corroles with electron-donating/withdrawing moieties has been prepared

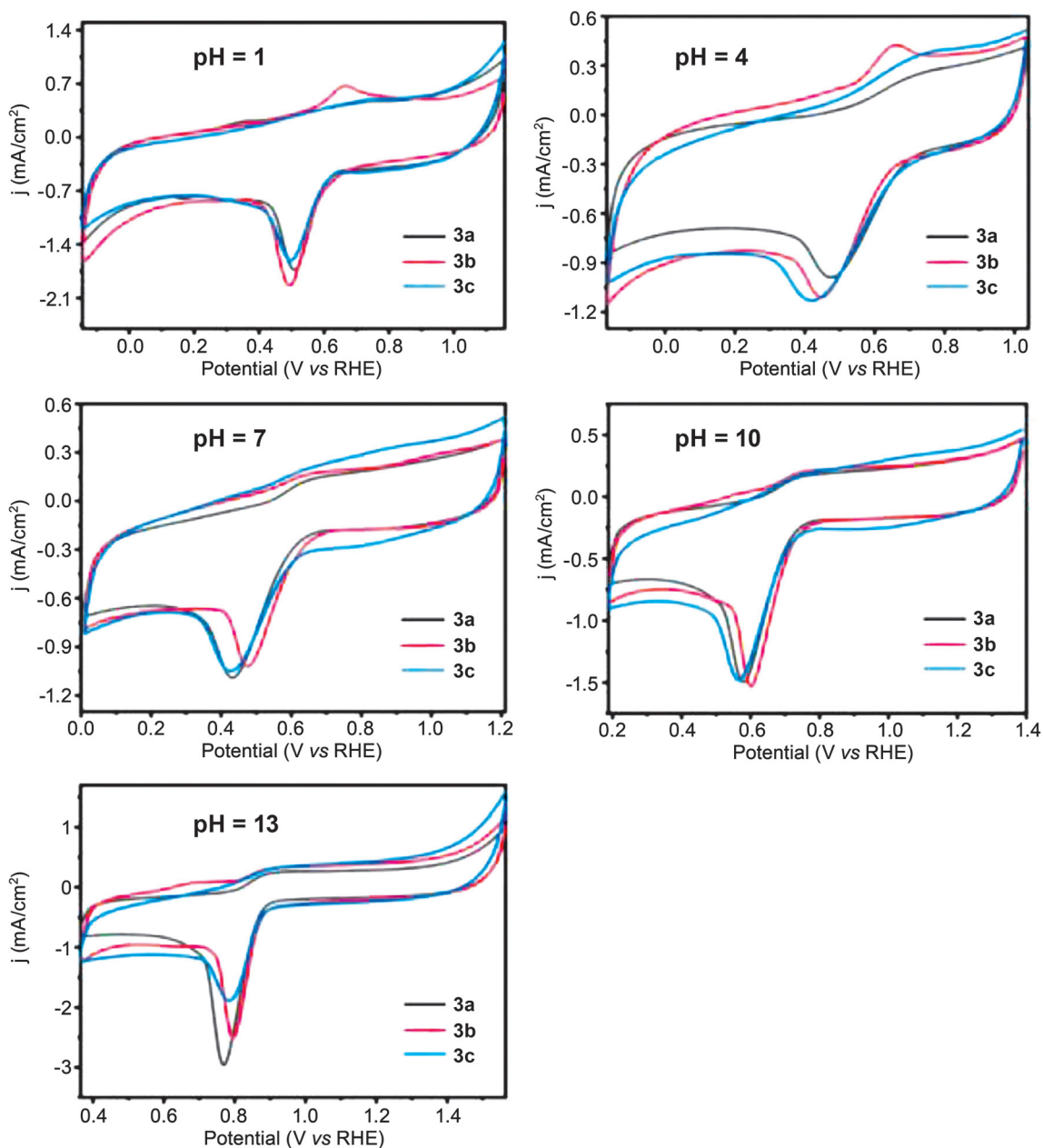


**Figure 5.** CV measurements of **3a-c** at various pH values under an O<sub>2</sub> atmosphere.

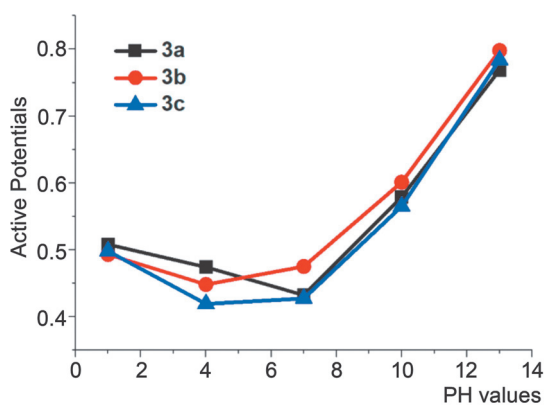


**Figure 6.** The active potentials vs pH values derived from CV measurements of **3a-c**.

and fully characterized. When different electron-donating and -withdrawing units were introduced at the *o*-positions of Co(III)-corroles, the influence on the tunable catalytic behavior can be assigned primarily to changes in the local environment since the inductive effects of the *o*-substituents are relatively weak. Considering super-structured metallo-corroles have a wide range of application, the current study will provide useful information for future molecular design related to enhanced electrochemically catalyzed energy-related small molecule activations.

**Acknowledgements.** This work was supported by the National Natural Science Foundation of China (21701058, 21703086), the Natural Science Foundation of Jiangsu Province (BK20160499), the State Key Laboratory of

Coordination Chemistry (SKLCC1817), the Key Laboratory of Functional Inorganic Material Chemistry (Heilongjiang University) of Ministry of Education, the China post-doc foundation (2018M642183), the Lanzhou High Talent Innovation and Entrepreneurship Project (2018-RC-105) and the Jiangsu University (17JJDG035). The theoretical calculations were carried out at the Centre for High Performance Computing in Cape Town. Dr. Wei Tang also acknowledges the financial support from Jiangsu Province (F201648) and the Zhenjiang Key Research Plan (SH2019055).

## References

- Ganguly S., Ghosh A. *Acc. Chem. Res.* **2019**, *52*, 2003–2014.
- Lim H., Thomas K.E., Hedman B., Hodgson K.O., Ghosh A., Solomon E.I. *Inorg. Chem.* **2019**, *58*, 6722–6730.
- Ghosh A. *Chem. Rev.* **2017**, *117*, 3798–3881.
- Buckley H.L., Rubin L.K., Chrominski M., McNicholas B.J., Tsen K.H.Y., Gryko D.T., Arnold J. *Inorg. Chem.* **2014**, *53*, 7941–7950.
- Guo Y.X., Gu T.T., Li P.F., Fu B., Sun L., Zhu W.H., Xu H.J., Liang X. *Inorg. Chem. Acta* **2019**, *496*, 119067.
- Petrova D.V., Semeikin A.S., Berezina N.M., Berezin M.B., Bazanov M.I. *Macroheterocycles* **2019**, *12*, 119–128.
- Kosa M., Levy N., Elbaz L., Major D.T. *J. Phys. Chem. C* **2018**, *122*, 17686–17694.
- Levy N., Mahammed A., Kosa M., Major D.T., Gross Z., Elbaz L. *Angew. Chem. Int. Ed.* **2015**, *54*, 14080–14084.
- Liang X., Niu Y.J., Zhang Q.C., Mack J., Yi X.Y., Hlatshwayo Z., Nyokong T., Li M.Z., Zhu W.H. *Dalton Trans.* **2017**, *46*, 6912–6920.
- Niu Y.J., Li M.Z., Zhang Q.C., Zhu W.H., Mack J., Fomo G., Nyokong T., Liang X. *Dyes Pigm.* **2017**, *142*, 416–428.
- Barata J.F.B., Neves M., Faustino M., Tome C., Cavaleiro J. *Chem. Rev.* **2017**, *117*, 3192–3253.
- Zhang X.F., Wang Y., Zhu W.H., Mack J., Soy R.C., Nyokong T., Liang X. *Dyes Pigm.* **2020**, *175*, 108124.
- Berezina N.M., Bazanov M.I., Maksimova A.A., Semeikin A.S. *Russ. J. Phys. Chem. A* **2017**, *91*, 2377–2382.
- Zhu W.H., Huang T.T., Qin M.F., Li M.Z., Mack J., Liang X. *J. Electroanal. Chem.* **2016**, *774*, 58–65.
- Berezina N.M., Thao V.T., Berezin D.B., Bazanov M.I. *Russ. J. Inorg. Chem.* **2017**, *62*, 1617–1621.
- Lei H.T., Li X.L., Meng J., Zheng H.Q., Zhang W., Cao R. *ACS Catalysis* **2019**, *9*, 4320–4344.
- Li H., Li X.L., Lei H.T., Zhou G.J., Zhang W., Cao R. *ChemSusChem* **2019**, *12*, 801–806.
- Stefanelli M., Pomarico G., Tortora L., Nardis S., Fronczek F.R., McCandless G.T., Smith K.M., Manowong M., Fang Y.Y., Chen P., Kadish K.M., Rosa A., Ricciard G., Paolesse R. *Inorg. Chem.* **2012**, *51*, 6928–6942.
- Friedman A., Saltsman I., Gross Z., Elbaz L. *Electrochim. Acta* **2019**, *310*, 13–19.
- Friedman A., Landau L., Gonen S., Gross Z., Elbaz L. *ACS Catalysis* **2018**, *8*, 5024–5031.
- Sinha W., Mahammed A., Fridman N., Diskin-Posner Y., Shimon L., Gross Z. *Chem. Commun.* **2019**, *55*, 11912–11915.
- Lai W.Z., Cao R., Dong G., Shaik S., Yao J.N., Chen H. *J. Phys. Chem. Lett.* **2012**, *3*, 2315–2319.
- Dogutan D.K., Stoian S.A., McGuire R., Schwalbe M., Teets T., Nocera F.G. *J. Am. Chem. Soc.* **2011**, *133*, 131–140.
- Dogutan D.K., McGuire R.J., Nocera D.G. *J. Am. Chem. Soc.* **2011**, *133*, 9178–9180.
- Li M.Z., Zhu W.H., Mack J., Mkhize S., Nyokong T., Liang X. *Chin. J. Struct. Chem.* **2017**, *36*, 367–380.
- Gouterman M. In: *The Porphyrins*. Vol. III, Part A (Dolphin D., Ed.) New York: Academic Press, **1978**. pp. 1–165.
- Michl J. *Tetrahedron* **1984**, *40*, 3845–3934.
- Mack J. *Chem. Rev.* **2017**, *117*, 3444–3478.

Received 26.01.2020

Accepted 06.05.2020